Environmental Science
Water Research & Technology

PAPER

View Article Online
View Journal | View Issue

Cite this: *Environ. Sci.: Water Res. Technol.*, 2025, **11**, 2608

Hydrolysis modeling for combined primary and RAS sludge fermentation at water resource recovery facilities

Leah Pifer,[a] Francesca Cecconi,[a] Fabrizio Sabba, *[ab] Bishav Bhattarai[a] and Leon Downing[a]

Water resource recovery facilities (WRRFs) across the country have implemented primary sludge (PS) and return activated sludge (RAS) fermenters to generate soluble carbon and volatile fatty acids (VFA) needed for biological nutrient removal (BNR). In this study, SUMO simulations were utilized to capture fermentation trends of PS and RAS, coupled with experimental data. Additionally, through this work, key parameters for modeling of hydrolysis were identified. The reduction factor for anaerobic hydrolysis (η_{HYD}), the yield of H_2 during fermentation, and the rate of methanogenic growth were found to be crucial parameters when modeling PS and RAS fermentation. Two different hydrolysis models were used to calibrate the experimental data, SUMO1 and a modified version of the SUMO1 model (SUMO1_mod); the latter as a dual hydrolysis model that distinguishes between slowly biodegradable COD from influent sources (X_B) and from endogenous biomass decay (X_{BE}). The results of this study showed that several factors in the overall hydrolysis rate equation changed with an increase in the proportion of PS blend. Firstly, with an increasing PS percentage, the product of the hydrolysis rate and η_{HYD} increased due to the higher X_B from influent, as opposed to the slower degrading X_{BE} from biomass decay. The best fitting anaerobic hydrolysis reduction factor and hydrolysis rate product shifted from 0.2 to 0.4 for the SUMO1 model, and 0.12 to 0.3 as a weighted average based on the PS/RAS ratio for the SUMO1_mod SUMO1 model. Additionally, the composition of the solids changed with an increase in PS percentage, resulting in a much lower proportion of heterotrophic biomass (X_{Het}) per g VSS but a higher X_B content per g VSS. Finally, the model structure changed as the solids composition changed, impacting the hydrolysis rate. With 100% RAS fermentation, both X_B and X_{Het} concentrations affected the rate following Monod-like kinetics. However, as the PS content increased, the model indicated that the rate kinetics might be influenced only by the X_{Het} content. This work provides guidance and a framework through which modeling can be used to predict fermentation rates that can be achieved through combined PS and RAS fermentation.

Received 10th June 2025,
Accepted 4th September 2025

DOI: 10.1039/d5ew00533g

rsc.li/es-water

Water impact

Water facilities optimize carbon management by blending primary sludge (PS) and secondary sludge (RAS) for enhanced nutrient removal and biogas production. Modeling studies using SUMO software identify key parameters for fermentation rate prediction, including anaerobic hydrolysis reduction factor and rate. Results show blending PS and RAS can boost rates to a limit, affecting nutrient release and process efficiency.

1.0 Introduction

Many water resource recovery facilities (WRRFs) across the United States have been impacted by increasingly stringent nutrient limitations while also facing pressure for resource recovery, recycling, and energy and chemical use reduction.[1,2] Harnessing the full potential of influent carbon is one major way that a WRRF can meet these drivers. Optimal carbon management at a WRRF can be achieved by diverting carbon rich feedstocks such as primary sludge (PS) and returned activated sludge (RAS) for beneficial use. For example, one potential use case for such carbon rich feedstocks is biogas production by feeding solids streams to anaerobic digesters to produce energy.[3]

A different potential use case for the diverted carbon is to help drive nutrient removal processes.[4,5] Biological nutrient removal (BNR) processes such as enhanced biological phosphorus removal (EBPR) and denitrification require carbon for optimal and stable operation. For wastewater where the

[a] *Black & Veatch, 11401 Lamar Ave, Overland Park, KS 66211, USA*
[b] *Department of Civil and Environmental Engineering, Syracuse University, Syracuse, New York 13244, USA. E-mail: fsabba@syr.edu; Tel: +1 315 443 4042*

influent carbon is not sufficient to drive the required BNR processes, WRRFs may seek the addition of external carbon sources such as methanol or MicroC®.[6] Different MicroC are available on the market; for example MicroC® 2000 is glycerin-based, and specifically applied as a carbon source for EBPR and other carbon-driven processes in wastewater treatment such as denitrification (**https://www.microc.com/products/microc-2000** – Environmental Operating Solutions, Inc, MA, USA). These external carbon sources however come with their own implicitly associated costs and environmental impacts.[7] Addition of external carbon sources also adds to the waste solids and sludge produced within a facility. Further, for EBPR specifically, having carbon in the form of simple chain volatile fatty acids (VFAs) accessible for polyphosphate accumulating organisms (PAOs) is needed for best performance.[5,8] As an alternative, fermentation of carbon rich sewage sludge can be utilized to provide the optimal VFA rich environment needed for such biological processes.

Fermentation is a multi-step metabolic process that converts complex organic compounds into simpler compounds. This process starts with enzymatically mediated hydrolysis from particulate slowly biodegradable chemical oxygen demand (COD) to readily biodegradable COD. The readily biodegradable carbon is then broken down through fermentation into VFAs by acidogenic bacteria. During the fermentation process, some of the COD can be lost due to hydrogen production.[35] The VFA can then be taken up by bacteria for denitrification or EBPR. If further digestion occurs, the VFA can also undergo acetogenesis and methanogenesis to transform into methane.[9]

Fermentate is the VFA rich product generated from fermenters, the reactors in which hydrolysis and fermentation take place. Fermentate has been proven to successfully drive many advanced BNR processes as an alternative to externally sourced carbon.[10] Multiple feedstocks can be used within a fermenter including PS, RAS, mixed liquor, and even fats oils and greases (FOG).[5] In some cases, other carbon-rich waste streams can be added to the fermenter to enhance the fermentation yield. One example of this is cranberry syrup waste fed to fermenters at Wisconsin Rapids Wastewater Treatment Plant to increase the expected fermentation yield.[11]

PS fermenters have been implemented at many WRRFs across the US for VFA generation. PS fermenters can be constructed in many different configurations. Depending on the configuration, this process can either require additional process units or can be retrofit into an existing plant.[5] While PS is a commonly implemented feedstock for fermentation, it does not come without a myriad of potential issues and considerations. Some of the largest drawbacks of PS fermenters are related to maintenance and operational issues of the fermenter. These issues can be related to corrosion, odor, and even toxic hydrogen sulfide formation.[12,13] The high solids content of the fermented primary sludge can sometimes limit how much can be used. This is because WRRFs clarifiers, used to settle out solids, have a limited capacity to handle the additional solids load.[14] An alternative feedstock which reduces these concerns is the fermentation of RAS.

RAS fermentation has also been implemented at many WRRFs across the US. One major drawback of RAS fermentation compared to PS fermentation is that the latter feedstock has generally been shown to have a higher hydrolysis rate for the associated particulate material.[3,16] It has been illustrated that adding a small fraction of PS can significantly improve fermentation rates achieved through RAS fermenters to combat this issue.[15] To further investigate the fermentation rates achieved with combined PS and RAS, Cecconi *et al.* 2024 (ref. 4) performed a series of fermentation experiments using various proportions of PS and RAS from multiple plants. The associated fermentation yields were tracked over 2 weeklong batch tests. While the product of this work highlighted many practical guidelines for combined PS and RAS, modeling of the experiments was not yet conducted to understand the mechanisms involved during combined PS and RAS fermentation.

Modeling using commercially available platforms such as SUMO (Dynamita, France) can both help validate results and predict fermentation performance at a WRRF. The focus of this modeling work was to shed light on the hydrolysis models available for fermentation, as this is commonly considered the rate-limiting step in the fermentation process.[17,18] To model hydrolysis, "surface-limited reaction kinetics" are frequently utilized. The hydrolysis rate of slowly biodegradable COD is known to vary depending on wastewater characteristics that encompasses different types of COD with disparate characteristics. To better characterize this large fraction, multiple dual hydrolysis models have been proposed and tested. Orhon, Çokgör,[23] for instance, broke up the slowly biodegradable COD hydrolysis into soluble (rapidly hydrolyzable) and non-soluble (slowly hydrolyzable) fractions. Other dual hydrolysis models that break up the slowly biodegradable COD fraction in a similar way have been proposed and tested by Drewnowski and Makinia[24] and Sollfrank and Gujer.[21]

Another dual hydrolysis model proposed by Ozyildiz *et al.* (2023)[3] breaks down the slowly biodegradable COD fraction into two sources: slowly biodegradable COD substrate from influent sources (X_B) and from endogenous biomass decay (X_{BE}). The variation in the rates of hydrolysis between PS and RAS have been reported in multiple studies and are provided in SI (SI2).[3,17,33,34]

Two different SUMO models were investigated in this study: SUMO1 and a modified version of SUMO1 (referred to herein as SUMO1_mod) based on the dual hydrolysis structure from the work of Ozyildiz *et al.* (2023).[3] Both the SUMO1 model and the SUMO1_mod dual hydrolysis models were tested using the PS-RAS fermentation experimental blends culminating from the work presented in this paper. These hydrolysis models were used to validate experimental results from Cecconi *et al.* 2024 (ref. 4) and evaluate the models' performance under different experimental scenarios. Finally, the hydrolysis model and its calibrated kinetic

parameters, determined in this work, were used to study a generic benchmark plant with the goal of investigating how the hydrolysis model dynamics shift with different PS and RAS proportions.

2.0 Materials and methods

2.1 Experimental approach

Batch fermentation experiments were conducted in duplicate polyethylene fermentation reactors, each with a working volume of 75 L. Batch experiments were conducted for approximately 2 weeks to ensure the full yield time series of all measured parameters was captured over the length of the experiments. Temperature of the reactors was maintained using a heating strip and temperature probe, set to 20 °C ± 2 °C (ITC-308, Inkbird Tech., China). Grab samples for primary analytes were collected three times a day for three days a week, spread out during the batch test to accurately characterize the time series of each parameter. Data were collected for the following parameters: VFA, total and soluble COD (TCOD and sCOD), ammonia (NHx-N), orthophosphate (PO_4^{3-}-P), and alkalinity. Total suspended solids and volatile suspended solids were also monitored throughout the week as per the standard methods for TSS/VSS.[16]

Batch fermentation experiments were conducted on various combinations of PS and RAS from two main WRRFs in Northern California. In this work "plant 1" was a longer SRT plant with a 7–11 day SRT range that conducted nitrification–denitrification operation. "Plant 2", instead, was a trickling filter facility followed by a solids contact basin with an SRT in the range of 2–3 days. PS from a third WRRF close to plant 2 was used as a surrogate PS for these experiments source due to the infeasibility of using plant 2 PS, as the solids content of the PS was too low. This third plant used as PS surrogate was selected due to its proximity to plant 2 and its similar influent characteristics and primary treatment performance to plant 2. For more information on the fermentation batch experimental setup as well as additional background on plant 1, 2 and the surrogate plant 3, detailed information can be found in the SI in the experimental setup section and in Cecconi *et al.* 2024.[4] Fig. S1 shows a schematic of the fermentation reactor setup, while Table S1 lists the analytical methods implemented as per Cecconi *et al.* 2024.[4] This study tested different mass proportions on each plant using combinations of PS and RAS. The proportions tested were (a) 100% RAS by mass, 0% PS by mass, (b) 50% RAS by mass, 50% PS by mass, (c) 10% RAS by mass, 90% PS by mass, and (d) 0% RAS by mass, 100% PS by mass.

2.2 Modeling approach

To model each experiment, a full plant mainstream liquid treatment model of plant 1 and plant 2 were calibrated in SUMO version 22.0.0 based on plant data that best reflected the period during which the respective experiments were conducted. The influent data used to calibrate each full plant model is shown in Table 1, with the relevant information for plant 3, the PS surrogate for plant 2, also provided. Plant 2 trickling filter data was added as well for context of the influent more directly going into the contact stabilization basin of plant 2.

The full plant model for each plant was simulated with constant inputs until steady state was achieved (approximately 14 days). After steady state, the relevant proportions of PS and RAS were sampled from the primary/secondary clarifiers in the full plant model into an SBR unit that mimicked the experimental conditions of the fermentation reactor. The SBR was then simulated in a batch mode for 2 weeks. The parameters of interest were extracted for comparison with the experimental results. The model kinetic parameters were primarily adjusted to match sCOD yield data observed during the experiments, with the NHx, PO_4^{3-}, TCOD, VFA, and VSS time series also used to assist in tuning the kinetic parameters. The experimental results from plant 1 were used to calibrate the fermentation model. The fermentation model was then validated with the experimental results from plant 2.

Once the kinetic parameters were adjusted based on the modeled fermentation from the first two plants, they were tested on a fermenter for a generic benchmark plant, using default SUMO influent plant characteristics. The benchmark plant was operated at an SRT of 2 days and 8 days to characterize both a short and long SRT operation. The benchmark plant model was tested with and without a selector zone in the mainstream treatment (*i.e.* a small unaerated zone at the beginning of the basin volume) to determine the impact such a configuration would have on the fermentation results. This selector zone was set at a relatively small fraction of the basin volume (10% of the overall volume). The solids inventories were adjusted to reflect average PS and RAS solids contents from literature. The fermenter unit in this model was set at a retention time of 2 days and operated as a flow-through fermenter instead of an SBR to better replicate the application at the full-scale plant. The model kinetic parameters from the calibrated batch experiment models were applied to this generic benchmark plant model. This generic benchmark plant model was used to determine how well the observed trends in the experimental results related to model results from a flow-through fermenter with average PS and RAS characteristics. It was also used to help understand how the impactful parameters in the hydrolysis models changed with different combinations of PS and RAS. Fig. 1A) and B) depict the plant 1 and plant 2 calibration model configurations, respectively, while Fig. 1C) illustrates the benchmark plant configuration with the flow-through fermenter.

2.3 Full plant model calibration

The calibration of influent fractionation was initially based on the daily operation data of the plant that reflected the influent during the period of the experiments. The fractions were subsequently adjusted so that the measured COD and solids data during the fermentation experiment were closely

Table 1 Influent data for plant 1, 2 and 3 (PS surrogate for plant 2) used for calibration of the main plant during experimental period. Plant 2 trickling filter effluent data also shown for context

Name	Units	Plant 1 (long SRT)	Plant 2 influent (short SRT)	Plant 2 trickling filter effluent	Plant 3
Flow	$m^3\ d^{-1}$	38 000	28 000	—	46 900
Total suspended solids (TSS)	$mg\ L^{-1}$	307	375	186	241
Biological oxygen demand (BOD)	$mg\ L^{-1}$	220	434	110	268
Total phosphorus (TP)	$mg\ L^{-1}$	5.5	6	6	6.1
Ammonia (NHx)	$mg\ L^{-1}$	31	33	30	33
Solids retention time (SRT)	Days	9	2	—	7

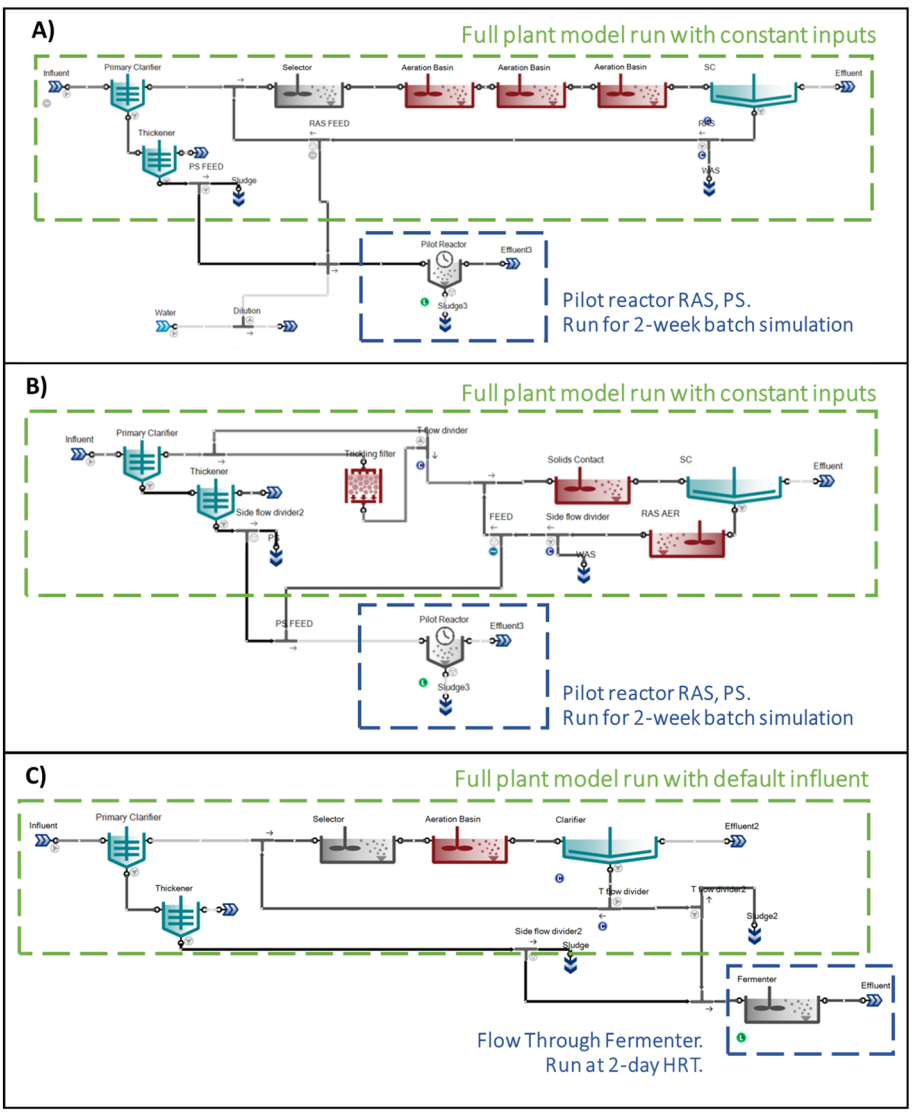

Fig. 1 A) Model configuration for plant 1 nitrification–denitrification facility, long SRT 8–10 days with SBR fermenter, B) model configuration for plant 2 trickling filter facility with solids contact basin, short SRT 1–2 days with SBR fermenter and C) model configuration for generic benchmark plant used to test calibrated kinetic parameters analysis with flow through fermenter.

aligned with what was observed in the model. Table S2 of the SI presents the final calibrated fractionation data utilized for the influent of plant 1 and plant 2. Throughout the experiments, the full plant model influent calibration for plant 1 and plant 2 were kept constant. The comparison between the plant influent data during the experimental periods as well as the model plant influent data can be seen in Table S3 of the SI. In addition, the full plant models were calibrated to ensure that the solids in the model corresponded to both the daily plant solids data and the experimentally determined RAS, PS, and starting fermenter TSS, VSS, and TCOD. The percent removal and concentration

of primary solids were modified to match the primary solids data. Furthermore, the flow to the plant model was adjusted to correspond to the MLSS and RAS solids. Table S4 in the SI illustrates the comparison between plant data and model-predicted values following model calibration. Maintaining a solids balance is important in fermentation modeling to ensure consistency in biomass representation for accurate simulation of process behavior.

2.4 Hydrolysis model structure

Following the calibration of the full plant models, the hydrolysis mechanisms and structure were then investigated in the model fermenter, with adjustments to kinetic parameters made locally within the process unit. Eqn (1) depicts the general rate equation for anaerobic hydrolysis of slowly biodegradable COD, with q_{HYD} representing the overall hydrolysis rate, η_{HYD} indicating the reduction factor applied for anaerobic conditions, and K_{HYd} representing the half saturation for hydrolysis of particulates. The last two terms in this equation relate to anaerobic hydrolysis inhibition from NOx and O_2, where $K_{NOx,OHO}$ and $K_{O_2,OHO}$ are half saturation constants for ordinary heterotrophs of NOx and O_2, and S_{NOx} and S_{O_2} are the soluble concentrations of NOx and O_2.

In this equation, hydrolysis is a function both of the slowly biodegradable COD (X_B) available as well as the heterotrophic biomass (X_{Het}) that produces the enzymes to mediate hydrolysis. When the X_B concentration is extremely low compared to X_{Het}, or $X_B/X_{Het} \ll K_{HYd}$, first order rate kinetics can potentially be assumed for hydrolysis with the rate being proportional to the X_B concentration.[17,19–21] If the opposite is true and the X_B concentration is much higher compared to X_{Het}, hydrolysis is no longer surface limited and hydrolysis is then proportional instead to the X_{Het} concentration.[22] In the case when neither is significantly higher, first order rate kinetics cannot be assumed and both concentrations impact hydrolysis.[17,19]

$$\frac{dX_B}{dt} = q_{HYD} \times \eta_{HYD} \times X_{Het} \times \frac{\frac{X_B}{X_{Het}}}{\frac{X_B}{X_{Het}} + K_{HYd}} \times \left(\frac{K_{NOx,OHO}}{K_{NOx,OHO} + S_{NOx}} \times \frac{K_{O_2,OHO}}{K_{O_2,OHO} + S_{O_2}} \right) \quad (1)$$

The typical ranges of the overall hydrolysis rate q_{HYD}, including the default values across process simulators are provided in SI (SI2). For the dual hydrolysis model structure of Ozyildiz *et al.* (2023)[3] that includes X_{BE}, a parallel rate equation exists for this respective slowly biodegrade COD source, with the respective hydrolysis rate associated with X_{BE} applied being the main difference in the equation.

3.0 Results and discussion

The next sections investigate a variety of aspects of the fermentation modeling conducted. The specific kinetic parameters that were found to be crucial for hydrolysis model calibration and their best-matching ranges are discussed. The subsequent performances of the calibrated models using SUMO1 and SUMO1_mod are then also presented. Lastly, the impact that solids concentration had on PS fermentation rate, how the hydrolysis kinetics changed with differences in PS/RAS fermentation, and additional practical insights on fermentation rate and nutrient release for PS/RAS blends are discussed, using both experimental results and the model outputs from the generic benchmark plant model.

3.1 Determination of major kinetic parameters

SUMO1 and SUMO1_mod models were matched to the experimental yield data observed during the study by adjusting the hydrolysis kinetic parameters, acetoclastic methanogen (AMETO) growth rate, and yield of H_2 during fermentation. The full range of kinetic parameters in the SUMO1 and SUMO1_mod models to match the experimental yield data can be seen in Table S5 of the SI.

For the SUMO1 model, the anaerobic hydrolysis reduction factor was adjusted instead of the hydrolysis rate itself, as anaerobic conditions were the focus of this study. The experimental yields primarily for sCOD were best matched by tuning the anaerobic hydrolysis reduction factor in a range between 0.14 to 0.2 for plant 1, and 0.1 to 0.2 for plant 2. The anaerobic hydrolysis reduction factor was much lower than the default for SUMO but was close to the range reported in the S2EBPR WRF report from 2023, where the best matching hydrolysis reduction factor for RAS fermentation ranged from around 0.05 to 0.15 for full-scale plants with SRTs less than 15 days.[22] This was also similar to the range of 0.11 to 0.3 as reported in Ozyildiz *et al.* (2023).[3]

For the SUMO1_mod model, the average anaerobic hydrolysis reduction factor of the blends from SUMO1 was first applied to the fermenter model for plant 1 at 0.18. The hydrolysis rates for X_{BE} and X_B hydrolysis were then modified separately to best match the experimental data across different blends. The hydrolysis rates themselves were adjusted instead of just the reduction factor for anaerobic hydrolysis to determine the respective rates for X_B and X_{BE} independently, since the reduction factor for anaerobic hydrolysis is present in both equations. Starting with the 100% RAS model, the hydrolysis rate for X_{BE} was determined to be best fitted at 0.67 d^{-1}, compared to the default value of 1 d^{-1}. Similarly, with the 100% PS model, the hydrolysis rate for X_B was determined to be best fitted at 1.68 d^{-1}, which was almost half the default of 3 d^{-1}. This set of kinetic parameters was then applied to plant 2 to assess how well the kinetic parameters matched the observed results without adjustment between plants. The same set of hydrolysis kinetic were applied across the different blends & two plants for the SUMO1_mod model in order to test the dual-hydrolysis structures adaptability. Additional details can be found in section SI 3 – Literature comparison of hydrolysis kinetics of the SI.

During the experiments, methanogenic activity was observed in the fermenter model, which was characterized by a declining sCOD yield around 10 days and an increase in methane production. This is a potential issue for fermenters, especially for PS, when the SRT of the fermenter is too long.[5] However, this uptake by methanogens was not observed based on the sCOD experimental data collected. It is hypothesized that this was likely due to small amounts of oxygen being entrained in the fermenter during the mixing process, as adding trace amounts of oxygen is a common way of combatting the onset of methanogenic uptake of the produced VFA in fermenters.[5,25] To account for this, slight reductions to the maximum specific growth rate of AMETO were implemented to match the overall shape of the sCOD yield curves, thereby avoiding the declining sCOD issue (ranging from 0.216–0.3 d^{-1}).

To better match the COD loss from the time series data and the observed NHx and PO_4^{3-} release, slight adjustments were made to the yield of H_2 production in fermentation with high VFA concentration as well. This parameter represents in SUMO the loss of COD to H_2 during fermentation. The best matching H_2 yield with high VFA concentration was in the range of 0.38–0.42 gCOD per gCOD for all the fermentation experiments, a slight adjustment from the default H_2 yield of 0.35. Further details around the calibration of this parameter can also be found in section SI 3.

3.2 Model performance with SUMO1 and SUMO1_mod

Fig. 2 shows the experimental sCOD yield data used to calibrate the SUMO1 and SUMO1_mod models during batch experiments for plant 1 long SRT, and plant 2 short SRT. All four experimental blends are shown with varying sCOD yields observed based on both their respective fermentation rates and initial VSS concentrations. The SCOD yield from the SUMO1 model calibrated for each experiment is represented as solid lines, while the dashed lines show the SUMO1_mod model calibration.

For both plant 1 and plant 2 data, the SUMO1 model was able to match the experimental data well but needed adjustment of the anaerobic hydrolysis reduction factor between experimental blends. The SUMO1_mod model was able to match plant 1 SCOD yields with similar accuracy to the SUMO1 model calibrations while keeping the same set of kinetic parameters across all blends. These same kinetic parameters from plant 1 SUMO1_mod model were then tested on the plant 2 data. It was observed that these kinetic parameters underpredicted the sCOD yields from the 100% RAS experiment and overpredicted the sCOD yields from the PS/RAS blend experiments for plant 2 data. While the SUMO1_mod model provided an advantage in hydrolysis calibration due to its adaptability between experimental PS & RAS blends for plant 1, these results indicate that the SUMO1_mod model was not similarly as adaptable between plants with disparate characteristics. Root mean square error (RMSE) describing the fit of the SUMO1 & SUMO1_mod models compared to the relevant experimental sCOD yield data are shown in Table S6 of the SI.

In addition to the differences between plant 1 and 2 and the experimental blends, the model performance was also investigated with respect to time. The two models were calibrated to match the overall sCOD saturation yields over the 2 week experimental timeframe. As is to be expected, the hydrolysis and fermentation dynamics were not constant through the whole range of the experiment. It was observed that a plateau occurred in the sCOD production of some experiments around the 7 day mark. This was most clearly observed for the plant 1 50% RAS 50% PS experimental results. This was likely due to a shift in the rate limiting step from being hydrolysis limited to biomass decay limited after X_B in the fermenter was depleted.[22]

It was also observed that all model results tended to underpredict the sCOD production at an experimental time of around 2–4 days using this method. This discrepancy in sCOD production could be due to the calibration focus on the full 2 week dataset. The first few days of experimental data are likely the most relevant due to the typical retention time for fermenters, in the range of 3–5 days for PS fermenter in the summer, and 3–4 days for a RAS fermenter.[5,25] The full 2 week dataset was still used for model calibration since

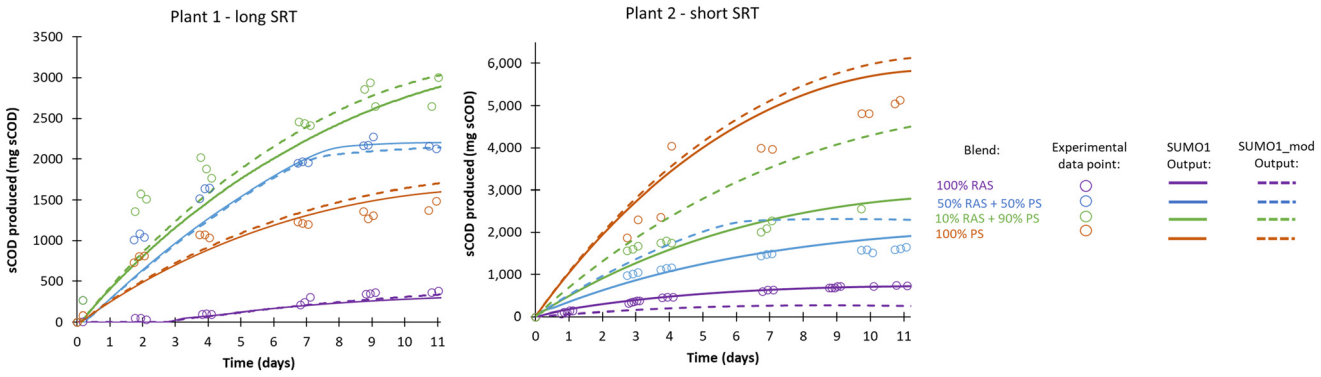

Fig. 2 sCOD yield data for plant 1 and 2 across different blends of batch experiments. Dots shown for experimental calibration data. Solid lines show calibrated SUMO1 model sCOD yield, and dashed lines show calibrated SUMO1_mod model sCOD yield.

control of retention time in full scale fermenters can generally be difficult depending on the fermenter configuration selected.[26] Using the full 2 week dataset is therefore more comprehensive to capture fermentation performance of a wide range of fermenter operating ranges.

For one of the batch experiments, a modeling check was performed in parallel and was calibrated to the first 2–4 days of experimental data. This modeling check resulted in an increase in the best matching anaerobic hydrolysis reduction factor by about 0.05 for both the SUMO1 and SUMO1_mod models, as compared to the full 2 week dataset calibration. Fig. S2 in the SI shows in greater detail the difference that could be expected with a shorter experimental data range selected for calibration. Future work could extend what was presented in this study to focus on the fermentation performance and modeling calibration in the 3–5 day SRT range of a typical well controlled fermenter.

3.3 Modeling fermentation at varying solids inventories

The characteristics of PS and RAS vary significantly between plants with different influent wastewater characteristics and different operational paradigm. One way in which these two sludge streams vary is in solids concentration, particularly VSS concentration. Table 2 shows typical ranges as well as extreme cases for PS and RAS total dry solids concentration (TS%), and the % of solids that is VSS. The typical VSS/TSS ratio for both PS and RAS is generally greater than 60%, however conditions such as wet weather storm events and or industrial loadings can influence this range to be as low as 40% for PS.[27] For WAS, low solids can also be common during operation of some plants particularly in developing countries, with VSS/TSS ratios at times $<50\%$.[28]

In Cecconi *et al.* 2024,[4] it was determined that fermenting the same RAS from plant 2 at concentration of 0.4% or 0.8% solids produced similar apparent fermentation rates per g of VSS in the reactor. This was determined to align with the assumptions of approximate first order hydrolysis kinetics, at least when investigating RAS with equivalent characteristics. The concentration of RAS is usually determined through mainstream BNR operational control (*i.e.*, SRT), rather than being controlled by fermenter operation. Therefore, the impact of RAS concentration on fermentation rate was not modeled.

Primary operation has a much larger range of operational strategies, and so the full range of PS solids content was varied through modeling to determine the effect on fermentation rate from 1% to 6% solids, as can be seen in Fig. 3. This was done on the generic benchmark plant model (using SUMO default inputs) using the kinetic parameters determined from the two calibration models with varying ranges of VSS/TSS ranges from literature. The fermenter model was run with a 2 day retention time in the flow through reactor as a steady state simulation. As shown in Fig. 3, the solids content had little effect on the normalized fermentation rate when the PS was greater than 2% solids concentration. The threshold after which the solids concentration no longer affects normalized fermentation rate may vary depending on the composition of the PS. In all simulations, the X_B content in the fermenter influent was much higher than the X_{Het} content, leading to the general applicability of first-order kinetics proportional to X_{Het}.

It was observed from the simulations that for solids concentrations less than 2%, there was a drop-off in apparent fermentation with lower VSS/TSS ratios. This supported the work of Banister *et al.* (1998), who found that for PS fermentation, there appears to be a fermenter solids concentration below which the fermentation potential yield appears to be limited.[30] This effect was even more apparent in the SUMO1_mod model results. Banister *et al.* (1998) also found an optimal range of primary sludge solids up to 2%. Some hypotheses about this behavior might be linked to a possible seeding effect or the biomass composition of the primary sludge. Banister *et al.* (1998) reported that increasing the seed population of facultative microorganisms, capable of acid fermentation, by adding partially fermented sludge to fresh primary sludge, significantly boosted VFA yields.[30]

3.4 Modeling hydrolysis with blended PS and RAS

The product of the SUMO1 model hydrolysis rate and reduction factor (anaerobic hydrolysis rate) from the plant 1 long SRT and plant 2 short SRT calibrations is plotted in Fig. 4A against the PS% mass in the blend. This ranged from 0.28–0.4 d^{-1} for the long SRT plant and 0.2–0.4 d^{-1} for the short SRT plant. The best fitting anaerobic hydrolysis rate increased with increasing PS% in the blend (by mass), similar to the results of Ozyildiz *et al.* (2023).[3] A linear

Table 2 Typical ranges of total dry solids (TS%) and volatile % of total solids in PS and RAS

	PS			RAS		
	Typical	Average	Extreme	Typical	Average	Extreme
Total dry solids (TS%)						
Metcalf & Eddy (2014)	1–6%	3%	—	0.4–1.2%	0.8%	—
Volatile dry solids as a percent of total dry solids (VS% of TS)						
Metcalf & Eddy (2014)	60–85%	75%	—	60–85%	70%	—
WEF (2018)[29]	64–93%	77%	—	—	—	—
WEF (2018)[29]	60–80%	65%	40%[a]	—	—	
Huang *et al.* (2019)	—	—	—	—	—	<50%[b]

[a] Caused by storm event or industrial loading. [b] Low solids exhibited in WAS of plants in some developing countries.

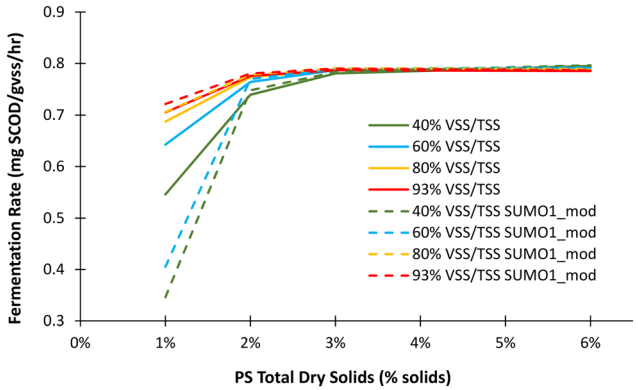

Fig. 3 Generic benchmark plant model results with calibrated kinetic parameters for fermentation of 100% PS at varying VSS/TSS% and solids concentrations in a typical range for PS. Solid lines show results of SUMO1 model and dashed lines show results of SUMO1_mod SUMO1 model.

relationship was fitted to the average from the two plants. For the SUMO1_mod model, the same set of kinetic parameters as determined for plant 1 were used across all blends. Fig. 4A also shows for the SUMO1_mod model the resulting product term of the hydrolysis rate and reduction factor for the proportions of X_B and X_{BE} hydrolysis occurring as the feedstock increases with PS content (weighted by the relative potions of RAS and PS mass at each blend). This value for the SUMO1_mod model ranged from 0.12–0.3 d^{-1}.

To better investigate the overall mechanisms of hydrolysis as they apply to an average facility, the effect of mass proportional blending of PS and RAS was investigated using both the SUMO1 and SUMO1_mod model on the generic benchmark plant model at both a short (2 days) and long SRT (8 days). The kinetic parameters determined from the fermenter model calibration of plant 1 and plant 2 were applied to the short and long SRT fermenter models respectively. For the SUMO1 model, the reduction factor for anaerobic hydrolysis was adjusted with PS% to reflect how this reduction factor increased with increasing % PS, as determined from the calibrated modeling results. The model was again run at a fermenter retention time of 2 days using steady state simulations for a flow-through reactor receiving varying RAS and PS fractions.

Based on these results, Fig. 4B shows the relationship between X_B and X_{Het} per g VSS as a function of the % (by mass) of PS in the blend for the short and long SRT results. Fig. 4B shows the results from the SUMO1 model. The SUMO1_mod model showed virtually the same results except that the particulate substrate was broken up into X_B and X_{BE} as well, which accounts for between 0.04 to 0.063 g COD per g VSS across all blends. It was observed that the X_B content per g VSS increased with PS% in the blend while the X_{Het} content decreased with PS% in the blend. Both parameters were then factors in the surface limited hydrolysis rate equation.

Fig. 4C shows that the proportion between X_B and X_{Het} increased with the % PS in the blend as well. X_B/X_{Het} was between 0.04–0.09 at the 100% RAS blend and increased to a

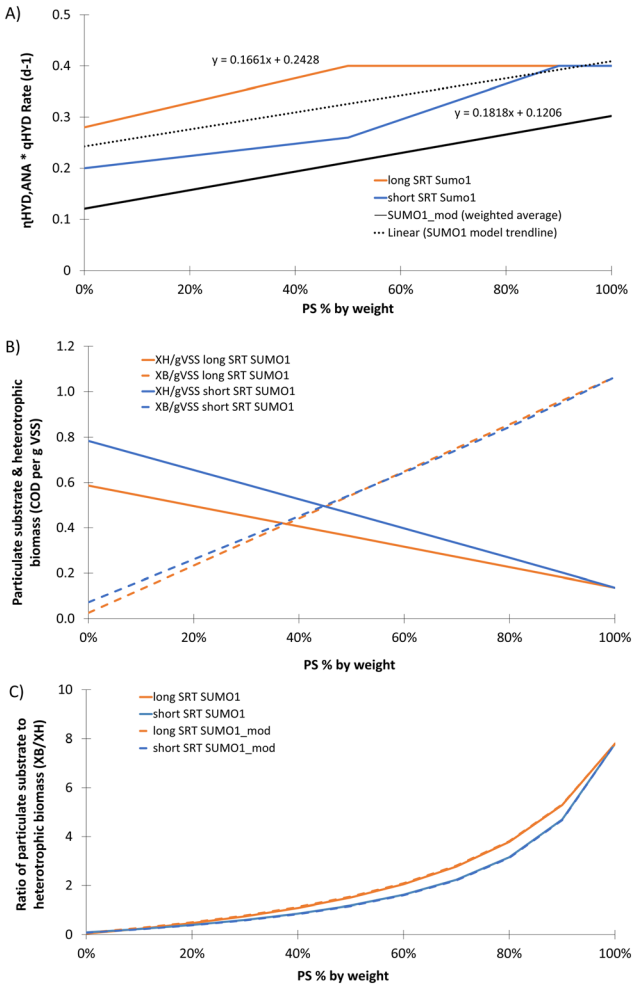

Fig. 4 A) Hydrolysis rate and reduction factor product of best fit for plant 1 and plant 2 model results for SUMO1. Linear trendline fitted to the hydrolysis data as dashed line. Black solid line indicates weighted average by weight for the SUMO1_mod model hydrolysis rate and reduction factor product. B) X_{Het} content per g VSS in the dashed lines with X_B content per g VSS in solid lines for the short and long SRT generic benchmark plant. Results shown for SUMO1 model but analogous in SUMO1_mod model results. C) Ratio of X_B to X_{Het} from SUMO1 and SUMO1_mod for short and long SRT of the generic benchmark plant model. All simulations for Fig. 4C were performed with K_{HYd} at SUMO default value (0.05).

ratio of about 7.8 at the 100% PS blend. The default value for K_{HYd} in SUMO was 0.05. There was therefore no blend for this generic benchmark plant model where $K_{HYd} \gg X_B/X_{Het}$, even at 100% RAS conditions. However, it was observed that at higher PS blends, when the X_B was much higher than X_{Het}, proportionality to the X_{Het} concentration could potentially be more applicable (*i.e.*, when $X_B/X_{Het} \gg K_{HYd}$ at higher PS% conditions as shown in WRF, 2019). This was investigated further in Fig. S3 of the SI.

The results of this study showed that several factors in the overall hydrolysis rate equation changed with an increase in the proportion of PS blend. Firstly, with an increasing PS percentage, the product of the hydrolysis rate and reduction factor increased due to the higher X_B from influent, as

opposed to the slower degrading X_{BE} from biomass decay. Secondly, the composition of the solids changed with an increase in PS percentage, resulting in a much lower proportion of X_{Het} per g VSS but a higher particulate substrate content per g VSS, particularly of influent X_B. Finally, due to the changing solids composition, the model structure itself appeared to change. Normal Monod-like kinetics where both X_B and X_{Het} concentration impact the overall hydrolysis rate are relevant with 100% RAS fermentation. However, with increasing PS content, the model suggested that rate kinetics proportional to only X_{Het} content were potentially applicable.

3.5 Practical implications of blended primary and RAS fermentation modeling

Fig. 5A compares the fermentation rates observed at varying proportions of PS (by mass) in a blend of PS and RAS, as determined experimentally and predicted by SUMO1 and SUMO1_mod models for the generic benchmark plant model. Both the modelling and experimental results showed that the 100% PS blend exhibited higher fermentation rates compared to the 100% RAS blend. It was observed that the generic benchmark plant model fermentation rates were lower than the experimental fermentation rates, particularly for the blends with higher proportion of PS. It was also observed from the generic benchmark plant outputs that the SUMO1_mod model predicted the trend of experimental fermentation rate with respect to PS% in the blend for the plant 1 experiments with similar accuracy compared to the SUMO1 model.

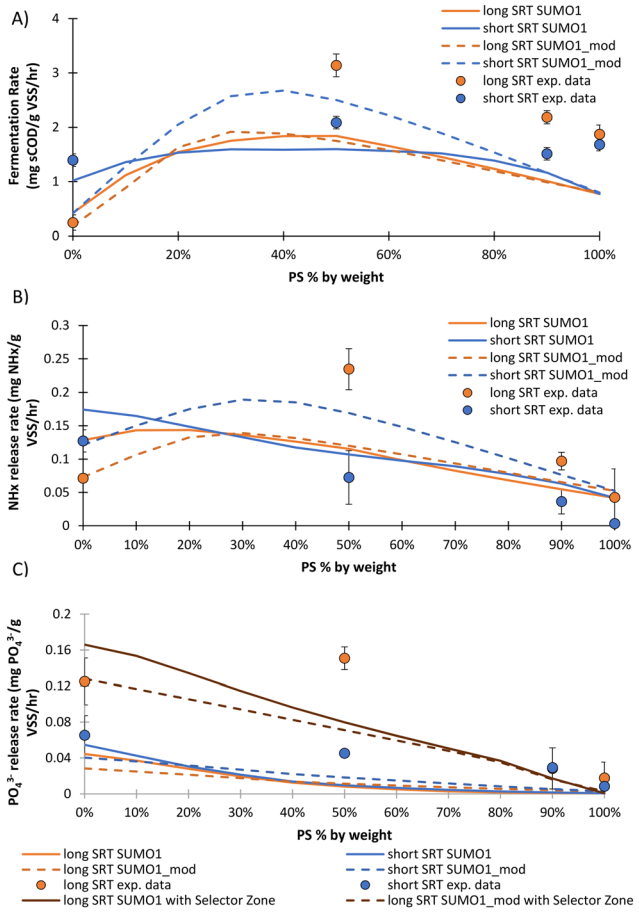

Fig. 5 A) Fermentation rate as a function of % PS content by weight. B) NHx rerelease per g VSS as a function of % PS in the blend by weight. C) PO_4^{3-} rerelease per g VSS as a function of % PS in the blend by weight PO_4^{3-} release shown with a generic benchmark plant model with and without a selector zone (and therefore PAOs). Experimental data shown as data points, solid lines show the SUMO1 model and dashed lines show the SUMO1_mod model. Both long SRT and short SRT shown.

Based on the fermentation rates observed in the experiment and the predictions from the generic benchmark plant model, it was evident that the addition of PS lead to an increase in the fermentation rate per gram of VSS, which was also demonstrated in other case studies.[15] Additionally, an optimum blend of PS and RAS between 30–50% PS by weight could exist, beyond which the fermentation rate per gram of VSS begins to decrease. The lower fermentation rates observed in the 100% PS blends compared to the blended fermentation rates were hypothesized to be attributed to higher starting VFA concentrations, lower pH of PS, and lower heterotrophic populations per gram of VSS that facilitates hydrolysis during the batch experiments.[4]

This last reasoning, with lower X_{Het} composition per gram of VSS, was supported by examining the results from the generic benchmark plant model shown in the previous section that discussed the hydrolysis modeling of RAS and PS blends. As the proportion of the PS in the blend increased, the hydrolysis model structure is potentially more proportional to X_{Het} content. This potential shift in hydrolysis structure applicability is in tandem with the X_{Het} concentration per gram of VSS decreasing for both the short and long SRT model results. Full-scale fermenter testing would help to further demonstrate the applicability of these model and batch testing results to real world applications.

Another consideration investigated in this work was the effect of PS on nutrient release. Nutrient release is linked to biomass decay during the fermentation process, which can potentially burden mainstream systems when EBPR and/or denitrification are applicable.[12,31] As discussed in Cecconi *et al.* 2024,[4] a lower proportion of RAS, and therefore lower biomass decay to produce the particulate substrate needed during fermentation, can help overcome this burden. Fig. 5B shows the NHx release as a function of PS% in the blend, while Fig. 5C shows the PO_4^{3-} release as a function of PS%. In all modeling, NHx and PO_4^{3-} were generally seen to decrease with increasing PS content in the blend per gram of VSS. For the SUMO1_mod model predictions as well as the long SRT plant experimental results, a maximum nutrient release per gram of VSS was observed with 30–50% PS in the blend of PS and RAS. While the fermentation rate per gram of VSS may be more optimal at a blend condition, it is possible that nutrient release could worsen. For a facility that has a major soluble carbon/VFA limitation, nutrient release

may be an unavoidable consequence of a necessary process but is still something to consider when managing stringent nutrient limitations.

One final consideration particularly for EBPR plants that have accumulated PAO, is that some of this phosphorus release may be related not just to biomass decay, but also P release associated with the uptake of VFA produced in the fermenter by PAO.[32] To better understand this, the benchmark model simulation results were compared between the model configuration with and without the small 10% volume selector zone in the full plant model, as discussed in the modeling approach section of the methods. Fig. 5C illustrates the impact of adding a small selector zone on PO_4^{3-} release. The effect of nutrient rerelease from RAS fermentation was observed through this exercise to be even more impactful for EBPR facilities with cultivated PAO populations.

4.0 Conclusions

This study aimed to investigate various hydrolysis models, determine the critical parameters for prediction, and evaluate model performance using both the experimental results and a generic benchmark plant model for combined PS and RAS fermentation. Two models, the SUMO1 model and the SUMO1_mod model, were determined to have similar accuracy when calibrated to the experimental data. These models had different state variables for X_B and X_{BE} from biomass decay and influent. It was found that the yield of H_2 with high VFA concentration had a major effect on the sCOD yield (adjusted to 0.38–0.42 gCOD per gCOD), as well as potentially the growth rate of methanogens for longer HRT fermenters (adjusted to 0.216–0.3 d^{-1}). The reduction factor for anaerobic hydrolysis ranged from 0.1 to 0.2 and increased with PS content due to the higher hydrolyzability. As a result, the anaerobic hydrolysis reduction factor and hydrolysis rate product ranged from 0.2 to 0.4 for the SUMO1 model, and 0.12 to 0.3 as a weighted average based on the PS/RAS ratio for the SUMO1_mod model. Practically, the modeling from this work also supported the conclusion that adding small proportions of PS sludge addition to the RAS fermentation significantly improved fermentation rates, up to a threshold of about 30–50% PS in the blend. Future work could focus on determining the applicability of these results to a full-scale flow-through fermenter, where biological communities may be structured differently from batch experiments, as well as on fermentation in the 2–4 day experimental range rather than spread out over the whole 2 week saturation curve of data collected in this study, as this shorter range is the retention time that most fermenters would be run if SRT is optimally controlled.

Glossary

AMETO	Acetoclastic methanogens
BNR	Biological nutrient removal
BOD	Biological oxygen demand
COD	Chemical oxygen demand
EBPR	Enhanced biological phosphorus removal
η_{HYD}	Hydrolysis reduction factor
H_2	Hydrogen
HRT	Hydraulic retention time
K_{HYd}	Half saturation for hydrolysis of particulate
$K_{NOx,OHO}$	Half saturation constant for ordinary heterotrophs of NOx
$K_{O_2,OHO}$	Half saturation constant for ordinary heterotrophs of O_2
MLSS	Mixed liquor suspended solids
NHx	Ammonia
NOx	Nitrate and nitrite
O_2	Oxygen
ORP	Oxidation reduction potential
PAOs	Polyphosphate accumulating organisms
PC	Primary clarifier
PO_4^{3-}	Orthophosphate
PS	Primary sludge
q_{HYD}	Hydrolysis rate
RAS	Return activated sludge
S2EBPR	Sidestream enhanced biological phosphorus removal
SBR	Sequencing batch reactor
sCOD	Soluble chemical oxygen demand
S_{NOx}	NOx concentration
S_{O_2}	O_2 concentration
SRT	Solids retention time
SUMO1_mod	SUMO1 modified
TCOD	Total chemical oxygen demand
TP	Total phosphorus
TSS	Total suspended solids
VFA	Volatile fatty acids
VSS	Volatile suspended solids
WAS	Waste activated sludge
WRRFs	Water resource recovery facilities
X_B	Particulate substrate
X_{BE}	Endogenous biomass decay
X_{Het}	Heterotrophic biomass

Conflicts of interest

There are no conflicts to declare.

Data availability

Supplementary information: The SI contains the following sections: fermentation batch test experimental methods, model calibration parameters, literature comparison of hydrolysis kinetics, model calibration to different time ranges of experimental data, further investigation of model structure variation with different ratios of PS and RAS. See DOI: **https://doi.org/D5EW00533G**.

The data supporting this article have been included as part of the SI.

Acknowledgements

We would like to express our gratitude to Black & Veatch's Innovation Platform for their support. We would also like to thank Jon Liberzon for the insightful discussions.

References

1 F. Sabba, Lab-scale data and microbial community structure suggest shortcut nitrogen removal as the predominant nitrogen removal mechanism in post-aerobic digestion (PAD), *Water Environ. Res.*, 2022, **94**(7), 10762.
2 P. McNamara, *et al.*, Post aerobic digestion (PAD) is a solids sidestream nutrient removal process that utilizes native carbon: performance and key operational parameters from two full-scale PAD reactors, *Environ. Sci.: Adv.*, 2022, **1**(2), 216–228.
3 G. Ozyildiz, *et al.*, Restructuring anaerobic hydrolysis kinetics in plant-wide models for accurate prediction of biogas production, *Water Res.*, 2023, **245**, 120620.
4 F. Cecconi, *et al.*, Improving carbon management through maximizing hydrolysis and fermentation at water resource recovery facilities, *Front. Environ. Eng.*, 2024, **3**, 1378621.
5 WRF, K. N. Abraham, Z. K. Erdal, W. K. Oldham, J. L. Barnard, J. B. Neethling, B. Rabinowitz and R. Baur, *Fermenters for Biological Phosphorus Removal Carbon Augmentation*, 2019.
6 C. Cherchi, *et al.*, Implication of using different carbon sources for denitrification in wastewater treatments, *Water Environ. Res.*, 2009, **81**(8), 788–799.
7 J. L. Willis, *et al.*, A greenhouse gas source of surprising significance: anthropogenic CO2 emissions from use of methanol in sewage treatment, *Water Sci. Technol.*, 2017, **75**(9), 1997–2012.
8 J. L. Barnard, Activated primary tanks for phosphate removal, *Water SA*, 1984, **10**(3), 121–126.
9 H. N. Gavala, *et al.*, Mesophilic and thermophilic anaerobic digestion of primary and secondary sludge. Effect of pre-treatment at elevated temperature, *Water Res.*, 2003, **37**(19), 4561–4572.
10 D. Kang, *et al.*, Redirecting carbon to recover VFA to facilitate biological short-cut nitrogen removal in wastewater treatment: A critical review, *Water Res.*, 2023, **238**, 120015.
11 F. Sabba, *et al.*, Enhancing resource recovery via cranberry syrup waste at the Wisconsin Rapids WRRF: An experimental and modeling study, *J. Environ. Manage.*, 2022, **323**, 116190.
12 J. Barnard, *et al.*, Fermentation of Mixed Liquor for Phosphorus Removal, *Proceedings of the Water Environment Federation*, 2010, vol. 2010, pp. 59–71.
13 J. L. Barnard, P. Dunlap and M. Steichen, Rethinking the Mechanisms of Biological Phosphorus Removal, *Water Environ. Res.*, 2017, **89**(11), 2043–2054.
14 E. Ossiansson, *et al.*, Primary filtration of municipal wastewater with sludge fermentation - Impacts on biological nutrient removal, *Sci. Total Environ.*, 2023, **902**, 166483.
15 L. Cavanaugh, *et al.*, A Small Footprint Approach for Enhanced Biological Phosphorus Removal: Results from a 106 mgd Full-scale Demonstration, in *Proceedings of the Water Environment Federation*, 2012.
16 R. B. Baird, A. D. Eaton and E. W. Rice, *Standard Methods for the Examination of Water and Wastewater*, American Public Health Association, American Water Works Association, Water Environment Federation, Washington D.C., 23rd edn, 2017, vol. 1, pp. 71–90.
17 V. A. Vavilin, *et al.*, Hydrolysis kinetics in anaerobic degradation of particulate organic material: An overview, *Waste Manage.*, 2008, **28**(6), 939–951.
18 P. L. Dold, G. A. Ekama and G. v. Marais, A General Model for the Activated Sludge Process, in *Water Pollution Research and Development*, ed. S. H. Jenkins, Pergamon, 1981, pp. 47–77.
19 D. Orhon, E. Ubay Çokgör and S. Sözen, Experimental basis for the hydrolysis of slowly biodegradable substrate in different wastewaters, *Water Sci. Technol.*, 1999, **39**(1), 87–95.
20 T. Mino, D. C. San Pedro and T. Matsuo, Estimation of the rate of slowly biodegradable COD (SBCOD) hydrolysis under anaerobic, anoxic and aerobic conditions by experiments using starch as model substrate, *Water Sci. Technol.*, 1995, **31**(2), 95–103.
21 U. Sollfrank and W. Gujer, Characterisation of Domestic Wastewater for Mathematical Modelling of the Activated Sludge Process, *Water Sci. Technol.*, 1991, **23**(4–6), 1057–1066.
22 WRF, L. Downing, A. Gu, P. Dunlap, Y. Tse, F. Sabba, J. Loconsole, I. Avila and J. L. Barnard, *Practical Considerations for the Incorporation of Biomass Fermentation into Enhanced Biological Phosphorus Removal*, 2023.
23 D. Orhon, E. U. Çokgör and S. Sözen, Dual hydrolysis model of the slowly biodegradable substrate in activated sludge systems, *Biotechnol. Tech.*, 1998, **12**(10), 737–741.
24 J. Drewnowski and J. Makinia, Modeling hydrolysis of slowly biodegradable organic compounds in biological nutrient removal activated sludge systems, *Water Sci. Technol.*, 2013, **67**(9), 2067–2074.
25 B. Rabinowitz, *et al.*, *Fermenters for biological phosphorus removal carbon augmentation*, 2011, vol. 9.
26 J. Chanona, *et al.*, Optimum design and operation of primary sludge fermentation schemes for volatile fatty acids production, *Water Res.*, 2006, **40**(1), 53–60.
27 Metcalf & Eddy, I., *et al.*, *Wastewater Engineering: Treatment and Resource Recovery*, McGraw-Hill Education, 5th edn, 2013.
28 X. Huang, Role of acid/alkali-treatment in primary sludge anaerobic fermentation: insights into microbial community structure, functional shifts and metabolic output by high-throughput sequencing, *Bioresour. Technol.*, 2018, **249**, 943–952.
29 F. Water Environment, *et al.*, *Design of Water Resource Recovery Facilities, Manual of Practice No.8*, Design of Water Resource Recovery Facilities, McGraw-Hill Education, New York, N.Y., 6th edn, 2018.

30 S. S. Banister and W. A. Pretorius, Optimisation of primary sludge acidogenic fermentation for biological nutrient removal, *Water SA*, 1998, **24**(1), 35–42.
31 P. Vale, *et al.*, RAS fermentation to enhance biological phosphorus removal, in *Proc. WEFTEC Conf.*, 2008.
32 F. Sabba, *et al.*, Impact of operational strategies on a sidestream enhanced biological phosphorus removal (S2EBPR) reactor in a carbon limited wastewater plant, *Sci. Total Environ.*, 2023, **857**(Pt 1), 159280.
33 G. Insel, *et al.*, A comprehensive evaluation of process kinetics: A plant-wide approach for nutrient removal and biogas production, *Water Res.*, 2022, **217**, 118410.
34 G. Kor-Bicakci and C. Eskicioglu, Recent developments on thermal municipal sludge pretreatment technologies for enhanced anaerobic digestion, *Renewable Sustainable Energy Rev.*, 2019, **110**, 423–443.
35 P. S. Barker and P. L. Dold, COD and nitrogen mass balances in activated sludge systems, *Water Res.*, 1995, **29**(2), 633–643.